Contrib Mineral Petrol (2016) 171:34
DOI 10.1007/s00410-016-1247-7

ORIGINAL PAPER

# Mt. Etna plumbing system revealed by combined textural, compositional, and thermobarometric studies in clinopyroxenes

**P. P. Giacomoni[1] · M. Coltorti[1] · J. G. Bryce[2] · M. F. Fahnestock[2] · M. Guitreau[3]**

Received: 16 June 2015 / Accepted: 2 March 2016 / Published online: 26 March 2016
© Springer-Verlag Berlin Heidelberg 2016

**Abstract** Coupled textural and in situ geochemical studies of clinopyroxene (cpx) phenocrysts, from both historical and recent eruptions of Mt. Etna volcano, provide a means to investigate the processes occurring in the deepest portion of the feeding system (>10 km depth). Five distinct textures were recognized: (1) normal oscillatory zoning, (2) normal zoning with Fe-rich rim, (3) sieve-textured core, (4) reverse oscillatory zoning, and (5) dusty rim. Electron microprobe analyses indicate an almost constant diopside–augite composition, with a slight enrichment in the enstatite for more recent erupted cpx. Core-to-rim compositional profiles, performed along the cpx, reveal distinct compositional characteristics. Normal oscillatory zoning is often characterized by a sharp increase in FeO ($\Delta$ ~ 2 wt%) accompanied by a drop in $Al_2O_3$ on the outermost 30 μm. Reverse oscillatory zoning, by contrast, exhibits a drop in FeO, $Al_2O_3$ ($\Delta$ ~ 2 wt%), and a remarkable crystal rim increase in MgO (up to 5 wt%). Similar compositional changes are evident in dusty-textured rims, which are characterized by dissolution edges and overgrowth containing glass pockets and channels. No significant compositional variations have been observed across crystals with sieve-textured cores. Trace element concentrations show enrichments in Sr, La, Zr, and REE, together with a decreasing La/Yb ratio (from ~7 to ~4) in rims of normally zoned crystals. Cpx with reverse zoning and dusty rims has low Sr, La, Zr, and REE contents toward crystal rims. Thermometers and barometers, based on equilibrium cpx-melt pairs, suggest that cpx cores start nucleating at 720 MPa, with the majority of them forming between 600 and 400 MPa but continuing to crystallize until very shallow depths (<100 MPa). Normal oscillatory-zoned phenocrysts surrounded by rims form at pressures shallower than 400 MPa, while reverse zoning and dusty rims occur between 400 and 500 MPa. Coupled petrologic and thermobarometric studies on both clinopyroxenes and plagioclases, associated with detailed textural and in situ geochemical analyses, are promising tools to reconstruct the entire magma ascent path beneath open-system volcanoes. At Mt. Etna, two distinct processes could account for the observed textures: Fe-rich rims in normal oscillatory-zoned crystals can be related to decompression-induced crystallization, while reverse zoning and dusty rims can be produced by mixing with a more basic magma at 400–500 MPa (i.e., ~10 km). Textural features are not restricted to a particular evolutionary phase of the volcano, which suggest that the deep feeding system has not changed significantly since the first alkaline volcanic phase.

**Keywords** Mt. Etna · Cpx phenocryst Textures · In situ trace elements · Geothermobarometers · Feeding system

Communicated by Gordon Moore.

**Electronic supplementary material** The online version of this article (doi:10.1007/s00410-016-1247-7) contains supplementary material, which is available to authorized users.

✉ P. P. Giacomoni
gcmppl@unife.it

[1] Department of Physics and Earth Sciences, University of Ferrara, Ferrara, Italy

[2] Department of Earth Sciences, University of New Hampshire, Durham, NH, USA

[3] Laboratoire Magma et Volcans, Université Blaise Pascal, Clermont-Ferrand, France

## Introduction

Numerous studies have demonstrated that Mt. Etna (Sicily, Italy) represents an important target for investigating magma dynamics in an open-conduit basaltic volcano. Despite its persistent activity, and long-lasting study, notably through well-developed monitoring networks, very few perspectives have been developed on the geometry of Mt. Etna feeding system, the localization of magma batches, and the mechanism(s) that triggered eruptions. In the last decades, particular attention has been focused on developing in situ geochemical techniques to measure elemental, and possibly isotopic, profiles across single minerals (e.g., Davidson et al. 2007; Ginibre and Wörner 2007), providing a means to develop more tightly constrained magma chamber and conduit processes leading to the onset of eruptions. Such techniques have already been applied to volcanic systems with different chemical affinity and from distinct geodynamic settings, as well as on both experimental materials and natural rocks. The results of such studies provided precious insights into pre-eruptive magma dynamics. Most investigations have focused on evolved systems such as Mt. St. Helens (Cashman 1988; Blundy and Cashman 2001, 2008), Mt. Parinacota (Ginibre et al. 2002; Ginibre and Wörner 2007), and Shiveluch volcano (Humphreys et al. 2006; Ferlito 2011). Comparatively, the few studies that have been dedicated to basaltic volcanic systems focused on Mauna Loa (Crisp et al. 1994), Stromboli (Landi et al. 2004), and Mt. Etna (Armienti et al. 1994, 2007; Viccaro et al. 2010; Kahl et al. 2011, 2013; Giacomoni et al. 2014; Mollo et al. 2015a).

Plagioclase is a frequently studied phenocryst because of its ubiquity in products, its sensitivity to temperature, pressure, and volatile content variations, as well as to the preservation of its chemical zoning and textures resulting from low NaAl-CaSi interdiffusion (Kuritani 1999; Davidson et al. 2007). Recent studies of chemical zoning and textures in plagioclases from Mt. Etna have highlighted the potential of this mineral in recognizing magma processes occurring within the feeding system, such as mixing and degassing (Viccaro et al. 2005, 2010; Giacomoni et al. 2012, 2014). However, the use of plagioclase is limited due to its crystallization at relatively shallow depths (<10 km; Lanzafame et al. 2013; Giacomoni et al. 2014; Mollo et al. 2015a; Vetere et al. 2015). Hence, we focus our attention on chemical zoning and textural features of clinopyroxene (cpx), which are a very common mineral phase in lavas from Mt. Etna since the early alkaline products of the Ancient Alkaline Centers (AAC) but also in lavas erupted by recent volcanic activity. Experimental studies (Métrich and Rutherford 1998; Mollo et al. 2011; Vetere et al. 2015) and pMELTS (Ghiorso et al. 2002) simulations (Armienti et al. 2004, 2007; Mollo et al. 2015a) have demonstrated that cpx forms as an early liquidus phase in conditions relevant to Mt. Etna. Cpx, in fact, crystallizes from a wide range of magmatic compositions and pressures, from mantle depths to the shallow feeding system (<10 km b.s.l.). For $H_2O$-rich magmas (>3 wt%; Métrich et al. 2004) of trachybasaltic composition, clinopyroxene is the first liquidus phase to crystallize at $P \geq 200$ MPa (Corsaro and Pompilio 2004; Armienti et al. 2007, 2013; Mollo et al. 2015a).

In this study, we focus on major and trace element compositions of cpx showing different textural features and representative of most of the volcanic activity of Mt. Etna from ancient (AAC) and prehistoric eruptions (Ellittico) to the recent eruptive events (2001, 2002–2003, 2006, and 2011–2012). Textures have been classified as 5 main types common to all eruptive periods. Thermobarometric calculations, performed to reconstruct the crystallization pattern of cpx during magma ascent, also helped to identify the physical–chemical variations that occur in the feeding system and determine the texture formation and chemical zoning. Integration of our cpx textural and thermobarometric studies with information deduced from plagioclase studies (Giacomoni et al. 2014) allows insights into the full spectrum of the Mt. Etna plumbing system to be gained.

### Geological evolution of Mt. Etna

Mt. Etna is a 3340-m-high stratovolcano located on the eastern coast of Sicily, covering an area of over about 1418 $km^2$ (Tanguy et al. 1997), and, with its continuous activity, represents the most important active volcano in Europe. The complex volcanic edifice is grown at the intersection of two major fault belts trending NNW–SSE (Tindari–Letojanni–Malta) and NNE–SSW (Messina–Giardini) and three structural domains: (1) to the north, the Peloritani mountain range corresponding to the Apennine–Maghrebian belt which extends westward; (2) to the south, the undeformed northern margin of the African plate constituted by the Hyblean Plateau and represents the foreland which plunges under the Catania–Gela foredeep; and (3) to the east, the Ionian lithosphere, considered to be a remnant of the Mesozoic Tethys (Monaco et al. 1997).

Volcanic activity in Etnean area started at about 500 ka (Gillot et al. 1994) with fissural and submarine volcanism that erupted olivine basalts with tholeiitic affinity (Fig. 1). Products erupted in this first stage (i.e., the Tholeiitic phase) likely constitute <10 % of the whole volume of emitted lavas. The Ancient Alkaline Centers (AAC) phase, which started at about 220 ka (Gillot et al. 1994; De Beni et al. 2005), corresponds to a time when lava compositions had shifted toward Na-alkaline affinity (Fig. 1). This was associated with a northwestward migration of the eruptive centers (Tanguy et al. 1997; Branca and Del Carlo 2004; Branca et al. 2008). The ancient products included several

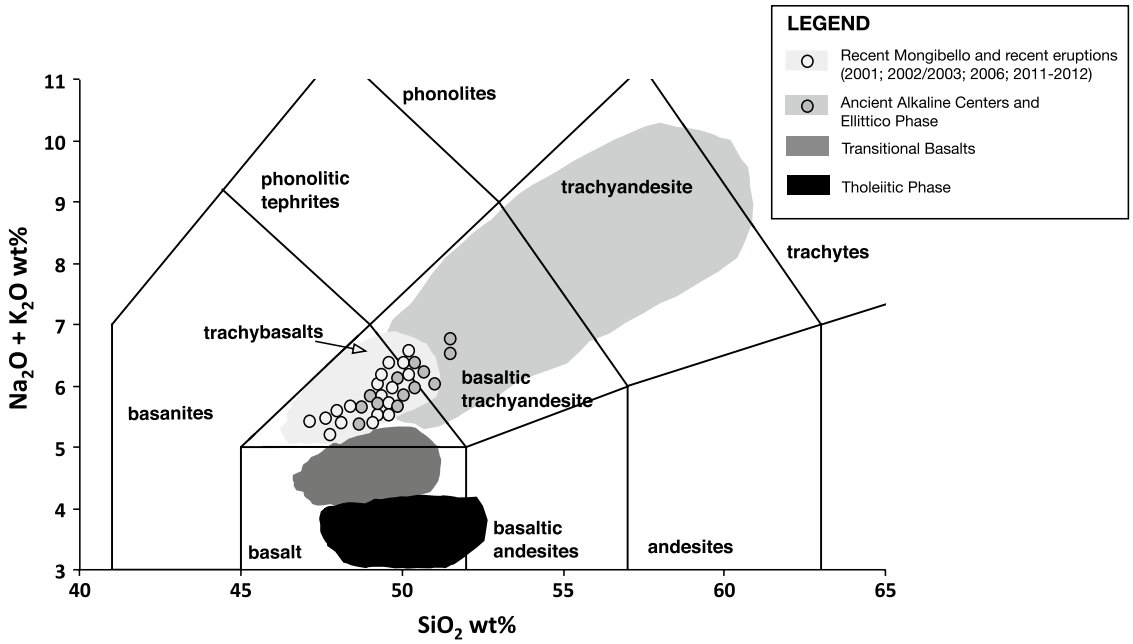


**Fig. 1** Total alkali–silica classification diagram (Le Maitre 2002) of erupted lavas from Tholeiitic, Transitional Basalts, Ancient Alkaline Center, Ellittico, and Recent Mongibello phases. Data are from this study (*circles*), Gillot et al. (1994), Tanguy et al. (1997), Métrich et al. (2004), Peccerillo and Lustrino (2005), Ferlito et al. (2009) and Giacomoni et al. (2012)

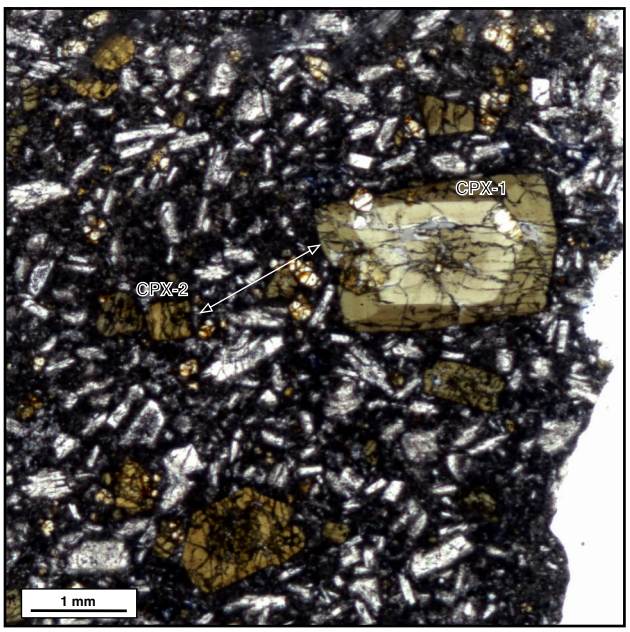


**Fig. 2** Thin sections representative of lavas from Ancient Alkaline Center eruptive phase. Two sizes of clinopyroxene, characterized by compositional zoning and sieve-textured core, can be distinguished

isolated volcanic centers that now crop out along the northern rim of the Valle del Bove. Many AAC lavas are characterized by large (>2 mm) cpx phenocrysts (Fig. 2). The Na-alkaline affinity has remained the dominant chemical signature of erupted products until recent time, with, however, different degrees of fractionation visible through time (Tanguy et al. 1997). During the Ellittico phase (60–15 ka), a large stratovolcano representing about 80 % of the current edifice formed, erupting both lavas and pyroclastic deposits (small ignimbrites and lahars), which cover a wide compositional range from hawaiite to trachyte (Fig. 1). About 15 ky ago, four plinian eruptions (Branca et al. 2008) partially destroyed the summit part of the Ellittico edifice that collapsed. Part of the emitted explosive material constitutes the Biancavilla ignimbrite, which crops out on the southeastern flank of the volcano. After the caldera formation, a shift toward basic compositions marked the beginning of the Recent Mongibello phase, which has continued until the present day. Ongoing activity occurs from the central craters (Bocca Nuova and Voragine), from three subterminal craters (South East and North East and New South East Craters), and from eruptive fissures along the S and NE rift systems. Emitted products mostly range in composition from hawaiite to mugearite, with some increase in K since 1971 (e.g., Tanguy et al. 1997; Schiano et al. 2001; Ferlito and Lanzafame 2010).

## Analytical methods

Samples from Ancient Alkaline Centers, Ellittico, Recent Mongibello, and Recent Eruptions (2001, 2002/2003, 2006 and 2011/2012) were collected from the freshest portions

of lava flows (Supplemental Table 1) and undergone petrographic study. Major and bulk rock trace element analyses were carried out at the laboratories of the Department of Physics and Earth Science of the University of Ferrara (Italy) on powdered aliquots of the lavas hosting the cpx samples. Whole-rock major and trace element concentrations were measured by X-ray fluorescence (Thermo ARL Advant XP) on pressed pellets. Voltages and energy varied depending on the atom weight of the element (30–60 kW, 50–100 A). Intensities were corrected for matrix effects using the method of Lachance and Traill (1966). Loss on ignition (L.O.I.) was determined by gravimetric method assuming $Fe_2O_3$ as 15 % FeO. Th, U, and REE were subsequently measured in solutions by inductively coupled plasma mass spectrometry (ICP-MS) on a VG Elemental PlasmaQuad 2Plus instrument. Accuracy and reproducibility for analyzed trace elements is in the range of 0.9–7.9 %. Conservatively, we shall assume an accuracy of 10 % and a detection limit of 10 ppb for U and Th.

Cpx major element abundances were determined in situ at the CNR-IGG, Section of Padua (Italy), using a Cameca SX-50 electron microprobe (EMP) equipped with four wavelength dispersive spectrometers (WDS) and one energy dispersive spectrometer (EDS). Cpx phenocrysts were analyzed in transects from core to rim using 20 μm steps. Operating conditions consisted in 15 kV accelerating voltage, 15 nA beam current, peak counting times of 15 s, and ~2 μm focused electron beam. Precision achieved is better than 1 % for major elements and below 3 % for minor elements. Core-to-rim transects ($n = 250$) were carried out by EMP on a selection of cpx from AAC, Ellittico, and Recent Mongibello phases (including 2002–2003 eruption). Subsets of these (35 of >100) crystals were also evaluated for trace element profiles on the most representative phenocrysts for each recognized texture we identify in the following section. *In situ* trace element concentrations in cpx were determined using laser ablation inductively coupled plasma mass spectrometry (LA-ICP-MS) at the Department of Earth Sciences of the University of New Hampshire (NH, USA). In this study, we used a New Wave Research UP-213 laser coupled to a Nu Instruments AttoM high-resolution mass spectrometer. Laser repetition rate was set to 3 Hz, energy to 50 %, and spot size to 40 μm, which resulted in a fluence of ~10 J/cm$^2$. Ablation signal integration intervals were selected by inspecting the time-resolved analysis to ensure that no inclusions were present in the analyzed volume. Concentrations were determined by internal and external normalization to $^{43}$Ca and NIST SRM 612, respectively. MPI-DING reference glass ML3B-G (Jochum et al. 2006) was used as a quality check during LA-ICP-MS analyses, and obtained results indicate a reproducibility and accuracy of trace elemental concentrations of 7–12 % (Supplemental Table 2).

## Cpx petrographic features

Cpx is abundant in all samples and usually range in size between 0.3 and 4 mm. It occurs as isolated crystals or as crystal aggregates, together with olivine and Ti-magnetite, in glomerophyric textures. Cpx phenocrysts usually have two distinct apparent sizes which both occur in the same thin section. The large phenocrysts range from 2 to 4 mm in size, while small ones vary from 0.9 to 0.3 mm (Fig. 2). Large cpx phenocrysts can be classified in five main textures. Distinctive textures manifest themselves as changes in crystal color (which is significantly more marked than the pleocroism), i.e., composition, between core and rim, or by the presence of dissolution–regrowth textures.

We classify the distinctive textures into five types (Fig. 3a–e). *Type 1* consists of euhedral homogeneous or oscillatory-zoned phenocrysts that are light beige in color and show normal zoning, often oscillatory without any trace of resorption or dissolution (Fig. 3a). *Type 2* consists of euhedral direct oscillatory-zoned bear beige-colored cores surrounded by brown rims (Fig. 3b). *Type 3* consists of sieve-textured cpx, often having rounded cores characterized by glassy pockets and interconnected glassy or recrystallized channels, all surrounded by an overgrowth with normal oscillatory zoning (Fig. 3c). *Type 4* consists of phenocrysts containing dissolved greenish rounded cores with reverse zoning surrounded by a yellow-brownish overgrowth (Fig. 3d). And, finally, *Type 5* consists of cpx showing reverse zoning, with a dusty, beige core with normal oscillatory zoning surrounded by a dusty rim with dissolution edges. Glassy pockets and interconnected glass channels characterize the dusty rims. Precipitation of newly formed cpx with more Mg-rich composition is usually found in the dusty area (Fig. 3e).

## Cpx major and trace element compositions

The Etnean cpx plots almost exclusively into the diopside (Di) field of the conventional International Mineralogical Association (IMA) classification diagram (Morimoto 1988) (Fig. 4). A shift toward more enstatitic (En) compositions is evident in some cpx phenocrysts of the Recent Mongibello. *Type 1* oscillatory-zoned phenocrysts are chemically almost homogeneous. Generally, FeO, $Al_2O_3$, $TiO_2$, and CaO contents increase from core to rim: FeO = 7.47–7.94 wt%; $Al_2O_3$ = 4.05–5.99 wt%; $TiO_2$ = 1.36–1.85 wt%; CaO = 21.77–22.81 wt%. MgO, by contrast, decreases from 14.16 to 12.71 wt% while Mg# remains almost constant (from ~76 to ~73) (Fig. 5a and Supplemental Table 3). Trace elements do not show significant variations: Nb and Cr increase toward the rim but REE, Sr, and Zr only exhibit slight increases (Supplemental Table 4). *Type 2* normal oscillatory-zoned phenocrysts

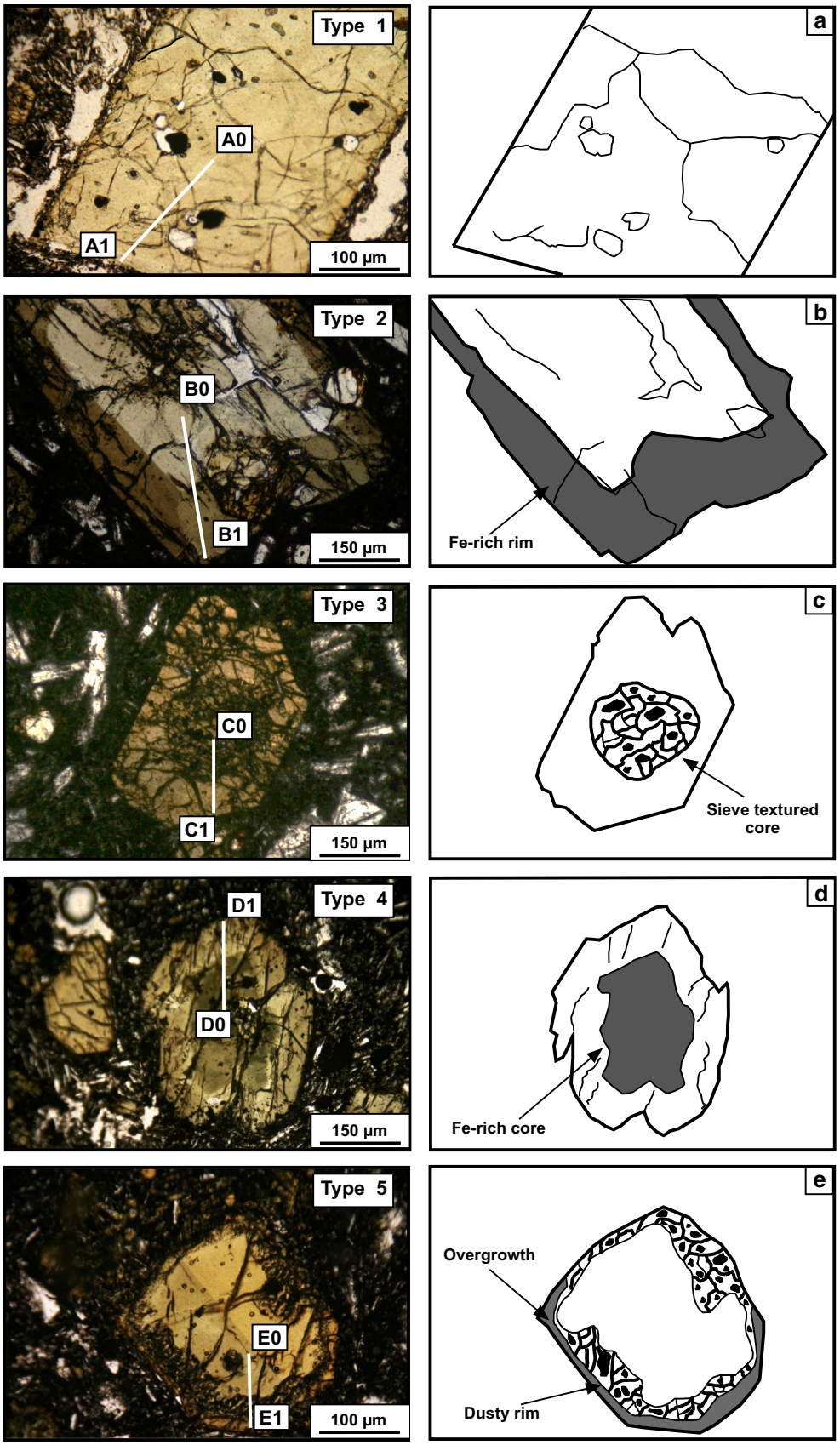


**Fig. 3** Photomicrographs and sketches of zoning and textures of cpx. **a** *Type 1* normal or oscillatory zoning; **b** *Type 2* zoning characterized by core-to-rim sharp compositional variation; **c** *Type 3* sieve-textured core; **d** *Type 4* reverse zoning; **e** *Type 5* dusty-textured rim with reverse zoning

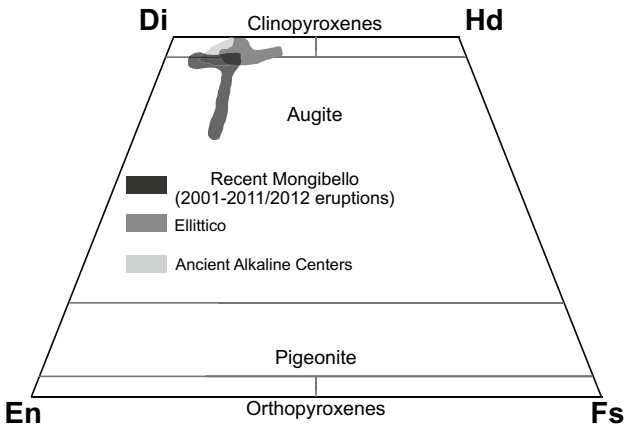


**Fig. 4** Composition of cpx at Mt. Etna classified using the Morimoto (1988) diagram. Di, En, Hd, Fs, and Wo stand for diopside, Enstatite, Hedenbergite, Ferrosilite, and Wollastonite, respectively

show a brownish rim with significant major and trace element variations (Fig. 5b). From core to rim: FeO content shows an abrupt increase from 4.04–6.16 wt% to 7.13–7.60 ($\Delta_{core-rim}$ > 2 wt% FeO on average), coupled with an increase in $Al_2O_3$ ($\Delta_{core-rim}$ > 3 wt% $Al_2O_3$ on average), and $TiO_2$ ($\Delta$ ~ 1.8 wt% $TiO_2$ on average). MgO and CaO, by contrast, both decrease from MgO ~17.0 to ~13.0 wt% and CaO from ~23 to ~22 wt%; similarly Mg# decreases in the FeO-rich zonation, changing from 84 to 78. Zr increases from 12.3 to 53.0 ppm, Sr from 74 to 111 ppm, and La from 1.73–1.81 to 7.22–7.78 ppm, while Cr decreases from 966 to 76 ppm (Fig. 6a and Supplemental Tables 3 and 4). *Type 3* phenocrysts with sieve-textured cores do not show any significant compositional variation in FeO, $Al_2O_3$, $TiO_2$, $Cr_2O_3$, or Mg# passing from the sieved area to the oscillatory-zoned overgrowth. Despite the remarkable and well-recognizable texture (Fig. 5c), only Sr, La, and Zr present a slight increase, while Cr and Nb decrease, similarly to *Type 2* phenocrysts (Fig. 6b—Supplemental Tables 3 and 4). Finally, *Type 4* phenocrysts, reverse-zoned phenocrysts without dusty rims, show a strong decrease in FeO from ~10.5 to 6.7 wt% and $Al_2O_3$ from ~7.6 to ~5.9 wt%. MgO increases from <10 to >13 wt%, similarly Mg# changes from 75 to 81. (Figure 5d); La, Sr, Zr, and REE decrease, while a strong enrichment is observed for Cr and Nb in the outermost parts of phenocrysts (Fig. 6c and Supplemental Tables 3 and 4). *Type 5* phenocrysts, reverse-zoned cpx with dusty rims, show a decrease in FeO from ~7.5 to ~6.6 wt% and $Al_2O_3$ from ~5 to ~3.2 wt%, coupled with an increase in MgO from ~13.3 to ~14.4 wt% and Mg# from 76 to 80 (Fig. 5e and Supplemental Tables 3 and 4). Trace element variations are similar to those recognized in Type 4 crystals (Fig. 6d and Supplemental Table 4). Notably, Eu contents vary from 1.30 to 2.59 ppm, in chondrite-normalized spider diagrams (Fig. 6), and the core and rim also show demonstrably distinctive behavior with respect to concentrations (Supplemental Table 4).

## Cpx-melt equilibrium conditions

Crystal-melt equilibrium conditions were checked before performing thermobarometric calculations on the basis of $^{cpx-liq}Kd_{Fe-Mg}$ between crystals cores, outer mantles and rims, and the whole rock (Supplemental Table 5) proposed by Putirka (2008), who experimentally determined an equilibrium value varying from 0.30 to 0.24 at $T$ > 1050 °C. Results from Ancient Alkaline Centers, Ellittico, and Recent Mongibello (2001, 2002–2003, 2006 and 2011–2012 eruptions) suggest that cpx compositions straddle the equilibrium range, with $^{cpx-liq}Kd_{Fe-Mg}$ values above or below the equilibrium conditions with respect to the host magma composition (Fig. 7).

Phenocrysts from Ancient Alkaline Centers have an average $^{cpx-liq}Kd_{Fe-Mg}$ of 0.29 (Fig. 7a). Some of them (~20 %) can be considered in equilibrium, although several samples are significantly more evolved ($^{cpx-liq}Kd_{Fe-Mg}$ = 0.31–0.4) or more Mg-rich ($^{cpx-liq}Kd_{Fe-Mg}$ = 0.22–0.16) compared to the host magma. Crystals from the Ellittico plot homogenously inside the equilibrium range (Fig. 7b), while cpx from 2001 and 2002–2003 eruptions plot significantly outside the equilibrium condition (Fig. 7c). For not equilibrated cpx from these eruptions, thermobarometric calculations were performed after the crystals were re-equilibrated with the most evolved magma composition emitted during the event (Fig. 7c, d; black crosses). Several crystals still remain outside the equilibrium condition even after recalculation and are considered as xenocrysts.

The majority of phenocrysts from the 2006 eruption plot slightly above the equilibrium range, with an average $^{cpx-liq}Kd_{Fe-Mg}$ = 0.34 (Fig. 7e). Re-equilibration calculation has been done by using a slightly evolved magma composition, erupted during the 2002/2003 event. The resulting cpx compositions have an average $^{cpx-liq}Kd_{Fe-Mg}$ of 0.26. The corrected cpx compositions have been used for thermobarometric determinations; some of the analyzed cpx must be considered as xenocrysts.

More than ~40 % of phenocrysts from the 2011–2012 event can be considered as in equilibrium with their host magma composition with average $^{cpx-liq}Kd_{Fe-Mg}$ = 0.28 (Fig. 7f and Supplementary Table S5). The existence, in the same lava flow, of phenocrysts within and outside the equilibrium range indicates a dynamic feeding system, where erupted magmas are able to incorporate crystals recycled from previous magma batches. This observation is in agreement with the model by Armienti et al. (2007) which propose the presence of that crystal mushes at different depths whose crystals may be incorporated into the uprising magma. Moreover, the presence of evolved cpx suggests

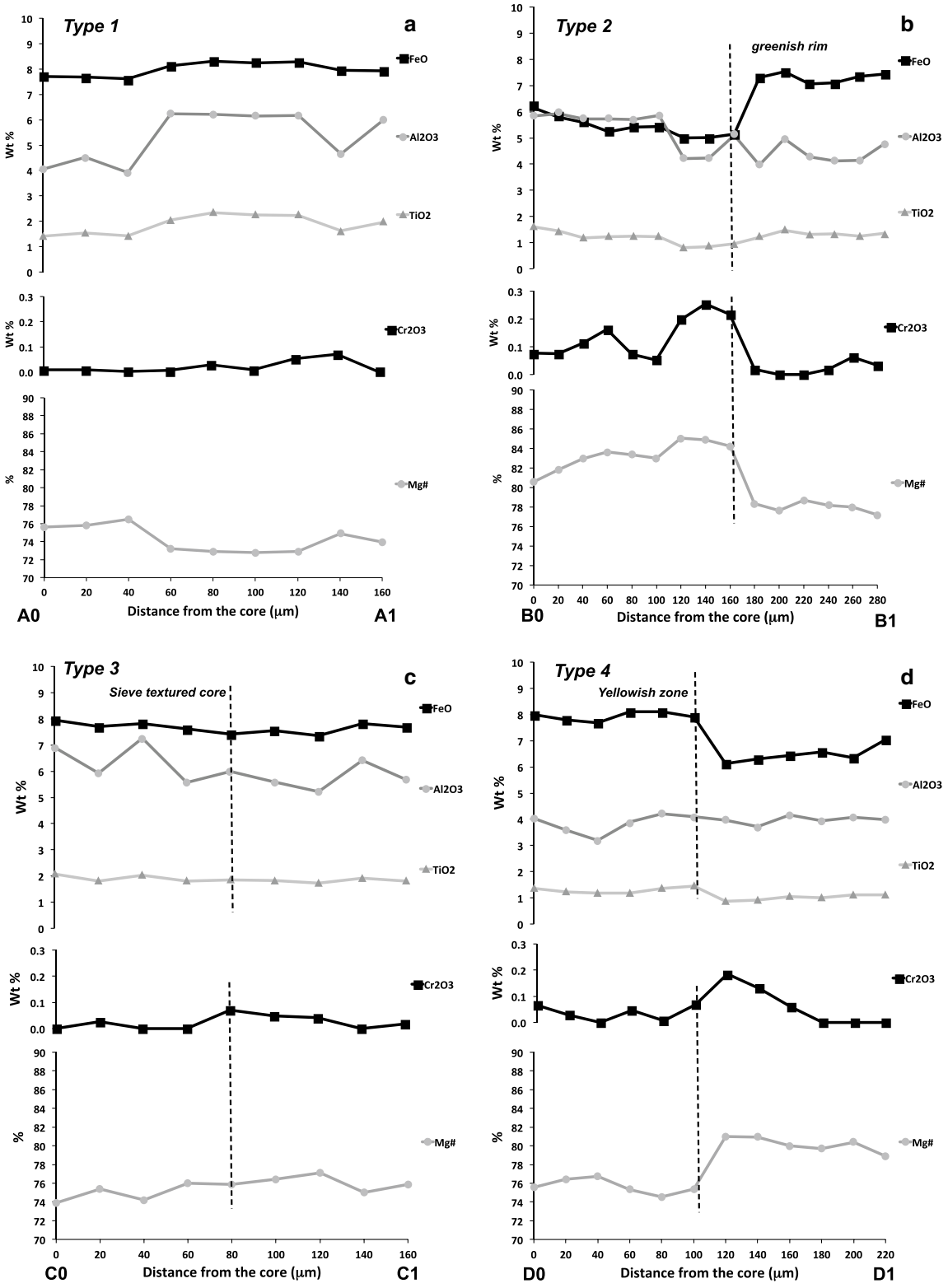


**Fig. 5** Major element (FeO, $Al_2O_3$, $TiO_2$) and $Cr_2O_3$ as weight percent (wt%) and Mg# [(Mg/Mg + Fe) * 100] compositional profiles of cpx phenocrysts from this study. **a** *Type 1*; **b** *Type 2*; **c** *Type 3*; **d** *Type 4*; and **e** *Type 5* zonations. Predicted error is <1 % for major and <3 % for minor elements; *error bar* is included in the symbol size

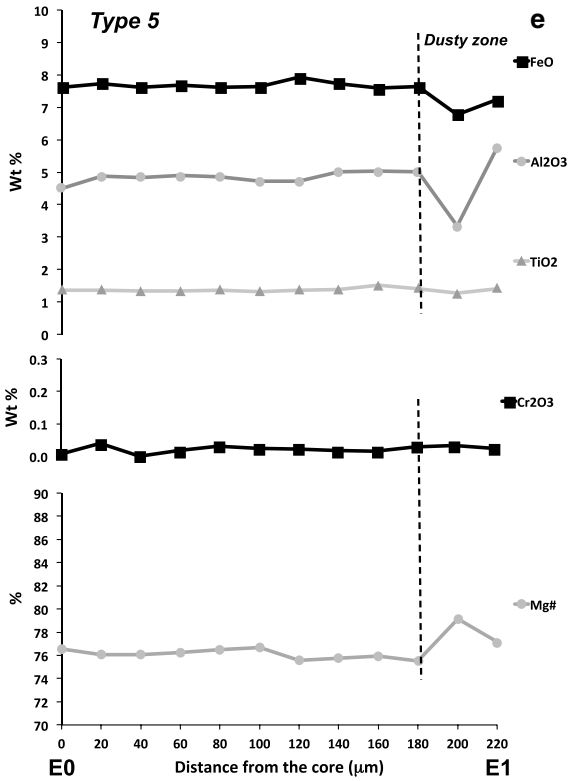


**Fig. 5** continued

that these crystals probably formed in a magma ponding in the upper portions of the feeding system, and have been entrained by a more basic magma soon before the eruption.

## Discussion

### P–T paths

Pressure and temperature crystallization conditions of cpx were determined for in-equilibrium and re-equilibrated cpx phenocrysts (283 cpx analysis) using the jadeite–diopside/hedenbergite exchange reactions (Putirka et al. 2003). This model is highly versatile with a standard error of estimate (SEE) of ±33 °C and ±170 MPa and has been applied successfully to numerous studies (Armienti et al. 2007, 2013; Mollo et al. 2011, 2015a; Jeffery et al. 2013). The phenocrysts and whole-rock compositions used for calculation are reported in the Supplementary Table S5. Calculations were performed by using the temperature, calculated with the P- and $H_2O$-independent equation of Putirka et al. (1996), in the barometer of Putirka et al. (2003). The water content was fixed at 1.5 wt% according to melt inclusion studies (Kamenetsky and Clocchiatti 1996; Métrich et al. 2004). It is worth noting that a change of ±1 wt% $H_2O$ is reflected in an error of ~15 bars, i.e., within the error bar of barometer. Resulting thermobarometric conditions indicate that studied cpx crystallized at pressures ranging from 750 to 160 MPa and over temperatures going from 1180 to 1070 °C. Results are plotted in Fig. 8, together with cpx from 1981 and 1991 eruptions (Armienti et al. 2007) and the position of the main crustal boundaries proposed by the CROP project (Finetti 2005). Despite studied phenocrysts plot at crustal pressure, cpx arguably crystallized from mantle depths to the subsurface over P–T paths mostly parallel to the curves that describe the pressure dependence of cpx liquidus temperatures, at different water contents (0–3 wt%), obtained through MELTS calculations (Ghiorso and Sack 1995; Armienti et al. 2007).

Most of the studied cpx started to crystallize at the Moho depth along the liquidus temperature corresponding to 1–2 wt% $H_2O$ in the melt (Fig. 8), and any systematic variations can be envisaged from most ancient (AAC) to the very recent eruptive products. Our results may be compared with those published in Armienti et al. (2013) who calculated P–T paths for both prehistoric (3930 BP and Monte Maletto) and historical (1669–2006) erupted products. Similarly, cpx crystallization essentially occurred from 700 to 160 MPa, the former corresponding to the Moho depth according to the density model of Corsaro and Pompilio (2004). Moreover, our results confirm that crystallization occurred in variably hydrated magmas, with

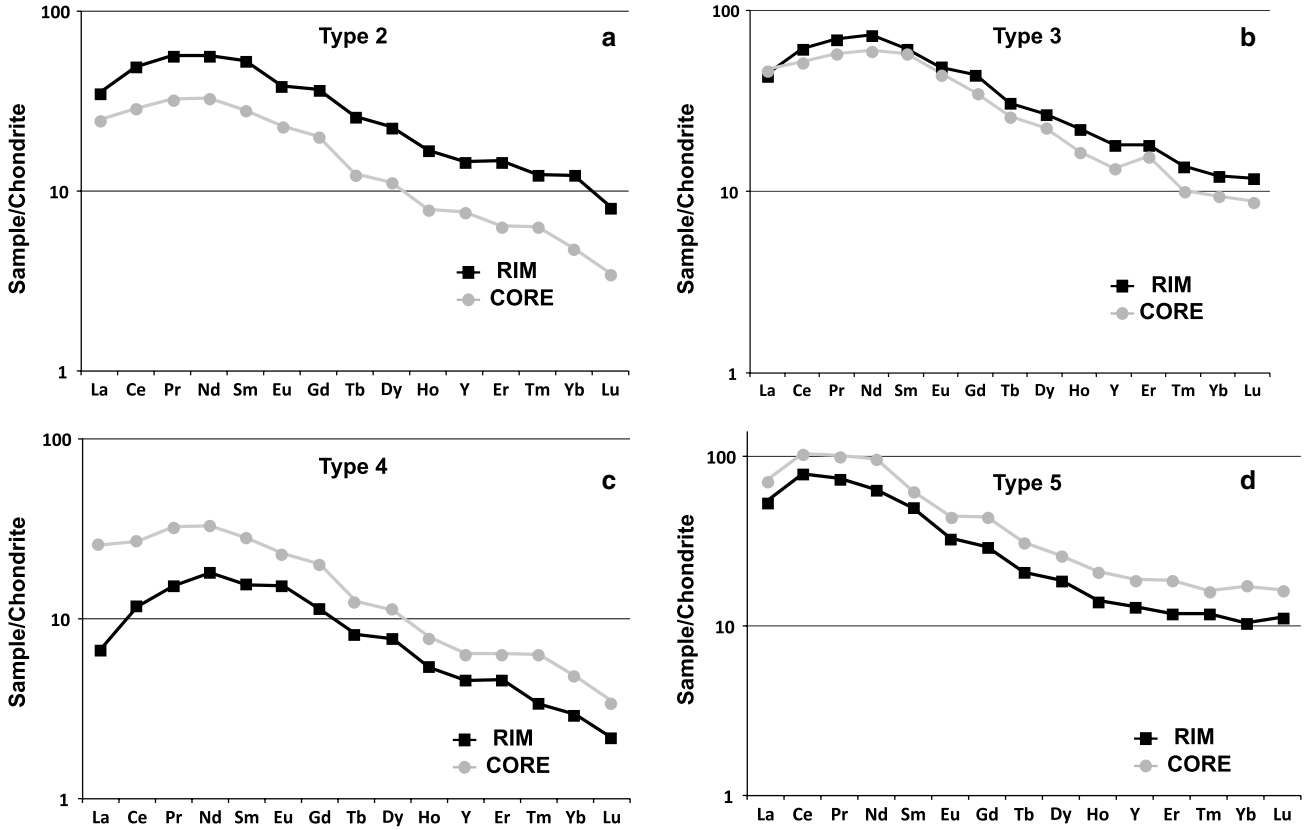


**Fig. 6** Chondrite-normalized (McDonough and Sun 1995) REE element spider diagrams in cores (*gray circles*) and rims (*black squares*) of studied cpx recognized on the basis of their textures: **a** *Type 2*; **b** *Type 3*; **c** *Type 4*; and **d** *Type 5* cpx

most of samples falling along the 1–3 wt% $H_2O$ liquidus line, without any correlation between $H_2O$ content and sample age. Among the studied cpx, those from the Ellittico eruptive phase plot along the most hydrated liquidus line, close to the 3 wt%, while the majority of the calculated P–T plot on the 1.5 wt% liquidus line (Fig. 8). Ascent rates appear very constant in the studied cpx, temperature loss varies from 42 °C/km in AAC; 43 °C/km for Ellittico, 60 °C/km for 2001, 45 °C/km for 2002/2003, 55.6 °C/km for 2006, and 52 °C/km for 2011–2012 eruption. Almost adiabatic ascent, as evidenced from Armienti et al. (2007) for the 1991 eruption data, has not been observed in samples from this study.

## Magma feeding system

Crystal-melt equilibrium conditions, thermobarometric estimates, and chemical–textural zoning are the result of complex processes occurring in the magmatic system, from crystal formation until eruption.

Disequilibrium is a common feature in the studied samples and can be used to recognize cryptic mixing buffered by whole-rock analysis (Mollo et al. 2015a). In this context, lavas are made up of a mixture of phenocrysts with different degree of disequilibrium: Some are in equilibrium with host magma, while other may have more primary or evolved features. This observation suggests that the erupted lava is a mixture of crystals from mushes equilibrated at different depth in the plumbing system, as also supported by Sr isotopes studies by Armienti et al. (2007) and crystal-melt disequilibrium of olivine phenocrysts (Kahl et al. 2011, 2013). Phenocrysts indicating more evolved compositions reasonably resided in the uppermost portion of the feeding system where massive degassing promotes magma undercooling, crystallization, and fractionation (Crabtree and Lange 2011; Mollo et al. 2015b). Phenocrysts must have time to re-equilibrate not magma. In such a dynamic scenario, phenocrysts in equilibrium with the host magma are those that remain enough time in contact with the melt in the main conduit or within lenses of magma to equilibrate.

The above-described scenario is common in most of the studied lavas suggesting that it is a main feature of an open-conduit basaltic volcano such as Mt. Etna, where magmatic recharge and eruptions are frequent. This is also supported by the fact that most compositions in disequilibrium where

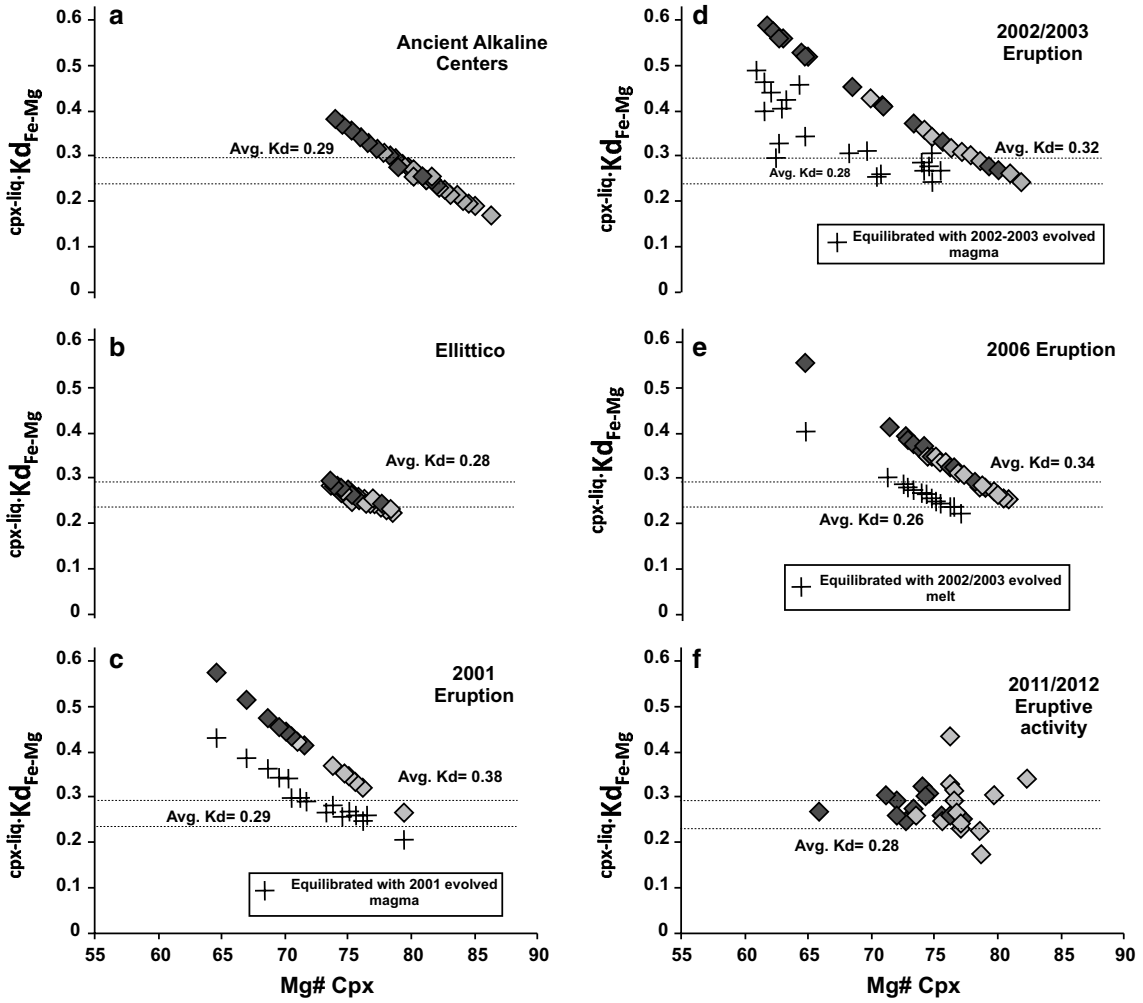


**Fig. 7** Mg# vs $^{cpx-liq}Kd_{Mg-Fe}$ of Ancient Alkaline Centers (**a**), Ellittico (**b**), 2001 eruption (**c**), 2002–2003 eruption (**d**), 2006 eruption (**e**), and 2011–2012 eruptive events (**f**). Equilibrium conditions for $^{cpx-liq}Kd_{Mg-Fe} = 0.24–0.30$ (Putirka 2008)

re-equilibrated simply using those of the lavas from the previous eruption.

Among the studied phenocrysts, only those from the Ellittico period (Fig. 7b) are homogeneous in composition and in equilibrium with their host magma supporting the hypothesis that a crustal magma chamber was present during this volcanic phase. In the Ellittico feeding system, cpx phenocrysts had enough time to equilibrate with the host magma with almost constant P–T conditions, somehow buffering the effect of the continuous magma injections.

Thermobarometric estimates for cpx phenocrysts, which have recognizable textural and chemical zoning, together with comparable data for plagioclase from Giacomoni et al. (2014), allow an assessment of the petrologic record of the Mt. Etna plumbing system to be made. Oscillatory zoning, frequent in Mt. Etna cpx as well as plagioclases (Duncan and Preston 1980; Giacomoni et al. 2014), has been attributed to diffusion and nucleation rates and/or to major changes in the physical and/or chemical conditions of the magma. Phemister (1937) first suggested that finer-scale oscillations are manifestations of local disequilibrium, while coarser oscillations arise from extensive chemical or physical changes within the magma body. Alternatively, small oscillations could result from diffusive disequilibrium at the crystal/melt interface in a fractionating magma batch. Such textural features could also be testimonies of cpx encounters, due to convection, with chemical and physical local heterogeneities inside the magma volume that can cause large-scale oscillatory zoning. The small compositional variations observed toward the rim for this type of crystal may be attributed to local chemical–physical heterogeneities in the feeding system that the crystal can encounter due to small dynamic convections. As an example, Gibb (1973) and Larsen (1976) attribute the entry of Na and $Fe^{3+}$ into cpx to small changes in oxygen fugacity ($fO_2$). $Fe^{3+}$ and Na migrate faster compared to other components, and

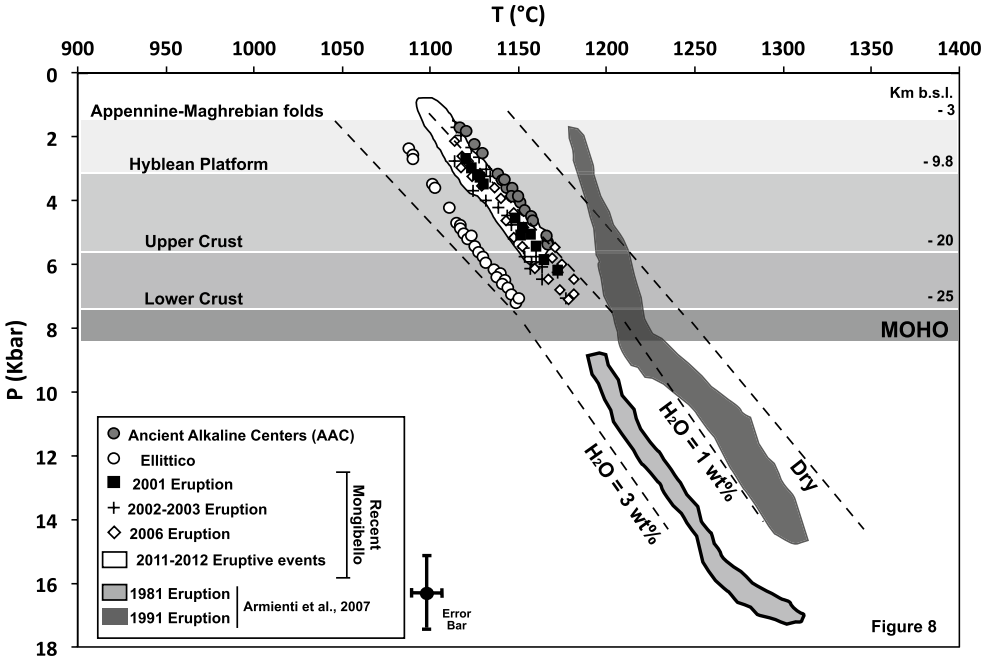


**Fig. 8** Temperature and pressure of crystallization of cpx calculated with geothermobarometers of Putirka et al. (2003) from Ancient Alkaline Centers (AAC), Ellittico, 2001 eruption, 2002–2003 eruption, 2006 eruption, and 2011–2012 eruptive phase. Data from 1981 and 1991 eruption from Armienti et al. (2007) are reported for comparison. Crustal stratigraphy is taken from Corsaro and Pompilio (2004), Moho depth is from Hirn et al. (1997). Curves calculated with MELTS code (Ghiorso and Sack 1995) represent the P–T conditions of clinopyroxene saturation for whole-rock composition with variable amount of dissolved $H_2O$

a local increase in $fO_2$ causes the chemical heterogeneities that may induce the migration by diffusion. The differential velocity of Na and $Fe^{3+}$, with respect to Ca and Mg, and/or $Fe^{2+}$ may thus account for the oscillating aegirina versus diopside components (Erikson 1985). *Type 1* crystals form along the entire magmatic column, from 790 to 250 MPa. An alternative interpretation comes from Mollo et al. (2013), which have demonstrated that, during the rapid growth of Etnean cpx, the crystal composition is progressively enriched in tetrahedral Al, Ti, and Na and depleted in $Fe^{2+}$, Ca, and Mg. The cpx chemistry is controlled by the substitution of M2 (Mg, $Fe^{2+}$) with M1 (Al, $Fe^{3+}$) coupled with the substitution of Si with Al in the tetrahedral site to form the Tschermak components. Highly charged cations, such as titanium and trivalent iron, are accommodated in the M1 site of clinopyroxene to balance the charge deficiency caused by the increase in the concentration of aluminum.

*Type 2* cpx are the most frequent Etnean texture. Their peculiar Fe-rich rims can be related to mixing with a more evolved melt or, as suggested by thermobarometric calculations, induced by decompression in an ascending and slightly fractionating magma column. The crystal cores formed from 590 to 300 MPa, while crystal rims nucleated in a very restricted depth range (200–300 MPa equivalent to 5–9 km below the summit craters, Fig. 9). *Type 3* sieve-textured cpx, by contrast, do not show significant chemical variations along the grain boundaries and in the subsequent re-growth, making difficult any attempt to interpret the texture. Analogies with similar texture experimentally reproduced in plagioclases (Iezzi et al. 2011) and studied in natural samples from 2001 to 2006 eruptive events of Mt. Etna (Giacomoni et al. 2014) suggest that sieve textures formed due to skeletal growth rather than by dissolution processes. The rare expression of such textures in Etnean cpx indicates that rapid growth conditions are unusual in the deepest portion of the feeding system, where cores start to nucleate. *Type 4* reverse-zoned crystals with iron-rich dissolved cores suggest an interaction with a more mafic magma. Dissolved rounded cores indicate that thermal erosion affected the pre-existing cpx at the contact with a more basic and hotter incoming melt. Such mixing event occurred just before the onset of the eruption and can be envisaged as the trigger mechanism. *Type 4* cores formed between 500 and 420 MPa (17–13 km below summit), whereas crystal rims formed between 390 and 190 MPa, with most of the determination plotting between 290 and 240 MPa (8–6 km below the summit) (Fig. 9). *Type 5* reversely zoned cpx with dusty rim have chemical variations similar to *Type 4* cpx. The occurrence of dusty textures indicate partial dissolution through reaction with a more Ca-rich and mafic magma. As found with plagioclase (Giacomoni et al. 2014), dusty textures in cpx are the direct expression of partial dissolution processes that result from an out-of-equilibrium interaction between a pre-existing core and a more mafic magma below liquidus temperature (Tsuchiyama 1985). Geobarometric determinations of *Type 5* depth of crystallization indicate that cores formed between 590 and 510 MPa (20–17 km below the summit), whereas dusty rims formed between 280 and 230 MPa (7–5 km below the summit).

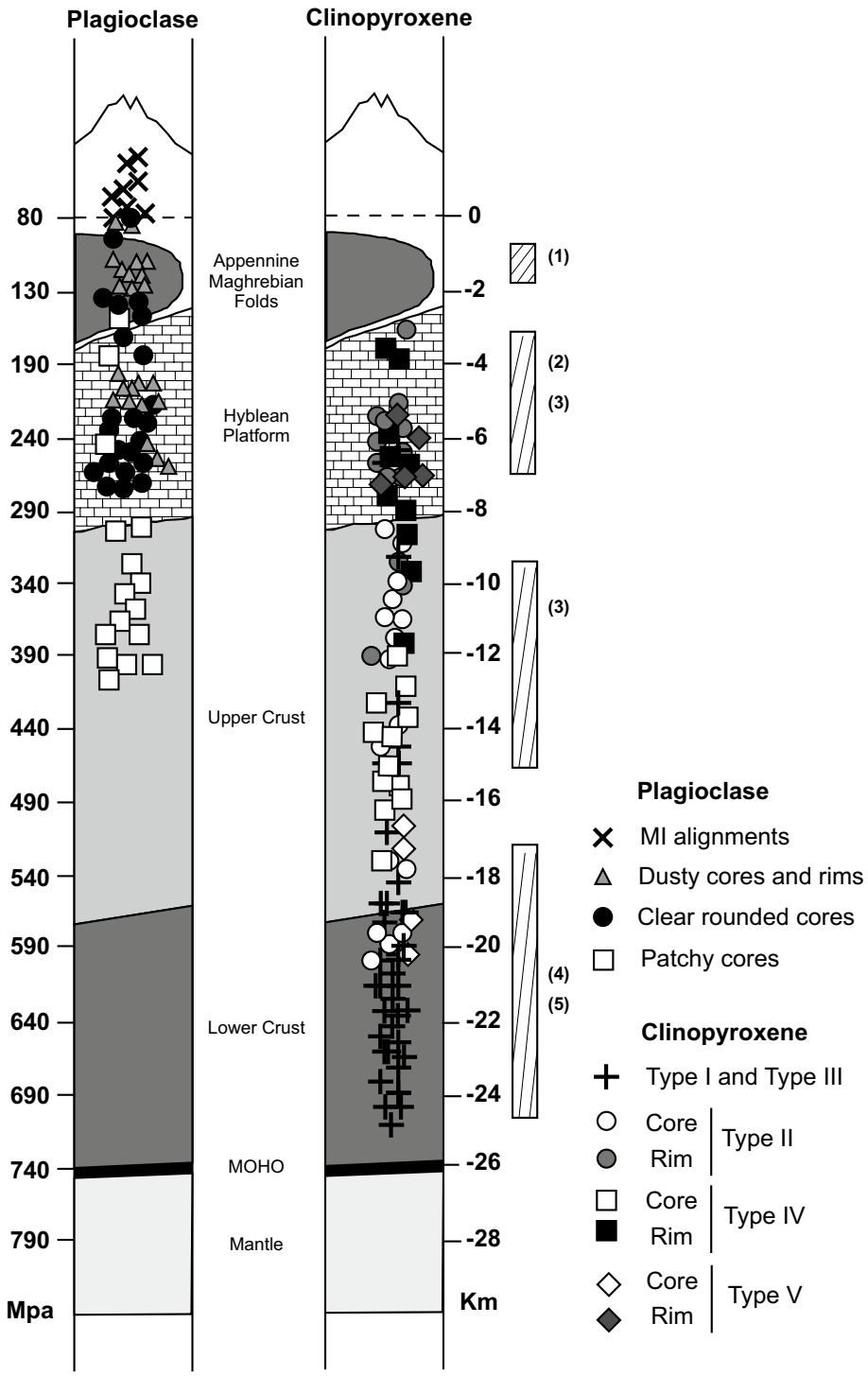


**Fig. 9** Sketched reconstruction of Mt. Etna volcano feeding system with depth of crystallization of main plagioclase (Giacomoni et al. 2014) and cpx textural groups (this study) at cores and rims. *Vertical bars* represent the range of depth of the tomographic low-velocity zones recognized by *1* Bonaccorso et al. (2011); *2* Lundgren et al. (2003); *3* Murru et al. (1999); *4* Sharp et al. (1980); *5* Patanè et al. (2013)

The comparison between plagioclase and cpx textural and compositional zoning (Fig. 9) suggests a homogeneous and continuous feeding system. Clinopyroxenes start to nucleate at mantle depths (28 km below the summit) and continue up to 4 km below the summit of Mt. Etna (Armienti et al. 2013). Evidence for deep crystallization from pressure determinations for 1981 and 1991 eruptions by Armienti et al. (2007), suggesting that clinopyroxene commonly forms at similar mantle pressure for the various volcanological evolutionary phases. These "deep" compositions are more rarely found in our thermobarometric survey. The deep crystallization pressures, yielded by the barometric data, are consistent with the lack of negative Eu anomalies in the core of most cpx, which in turn indicate that most the phenocrysts crystallized in deep portions of the feeding system where plagioclase is essentially absent.

Interestingly, *Type 2* cores bear no Eu anomaly, but rims show a negative shift, suggesting that they, respectively, crystallized out and within plagioclase saturation. By contrast, rims in *Types 4* and *5* cpx, determined by thermobarometry to have formed at shallower pressures, show slight positive Eu anomalies that are absent in the corresponding cores.

Complex reaction textures in cpx (*Type 2*, *Type 4*, and *Type 5*), which are similar to dissolved and dusty core and rims in plagioclase, formed in a restricted depth range (5–9 km below the summit). Most likely, the coincident pressure, determined from independent crystallization depth estimates for cpx and plagioclase showing complex reaction textures, reveals where magmas ponded last before the onset of eruptions. There, transiently residing melts frequently mixed with more basic and undegassed magmas that originated from greater depths.

Our thermobarometric interpretations based on geochemical signatures and textures are consistent with geophysical studies (Murru et al. 1999; Patanè and Privitera 2001; Patanè et al. 2006, 2013) documenting the absence of a long-lived magma chamber and, by contrast, identifying several magma ponding zones at 4–6 km b.s.l. and 8–12 km b.s.l using seismic tomography. Magma batches appear to stagnate more frequently at depths corresponding to the main discontinuity in crustal lithology, as indicated by seismic CROP study of Finetti (2005) and depicted in Fig. 9. These lithologies are (1) the Appennine Maghrebian to Hyblean Platform (130–150 MPa or ca. 2 km bsl) and (2) the Hyblean Platform to Upper Crust (~300 MPa or ~8 km bsl). This relationship between magma buoyancy and stagnation at main crustal discontinuities has been also reported in the study of Corsaro and Pompilio (2004).

The shallower magma ponding site is very close to the $H_2O$-saturation depth calculated in Giacomoni et al. (2014), which takes into account a variable amount of $H_2O$ in the basic magma (0.8–3 wt%). Mixing between deeper sourced undegassed magmas and shallower melts, close to $H_2O$-saturation depth, can be an efficient mechanism to trigger eruption through $H_2O$ exsolution. Moreover, the absence of plagioclase, together with observed positive Eu anomaly in cpx associated with crystallization at these depths (*Type 4* cpx rims as depicted in Fig. 9), indicates that lavas mostly crystallized in shallow portions of the feeding system due to volatile loss.

Studied phenocrysts and literature thermobarometric data did not show significant variations in the P–T of crystallization through their growth. These observations, coupled with the identification of the textural types of clinopyroxene throughout 200 ky of Etna volcanism, suggest that the deep portions of the feeding system did not vary significantly since the Ancient Alkaline phase. Additionally, the thermobarometry data suggest basic magmas start nucleating clinopyroxene from 1400 to 780 MPa depending on the initial $H_2O$ content.

## Conclusions

Textural and chemical features of cpx reveal processes occurring during magma ascent starting from the deepest part of Mt. Etna feeding system. This approach, when combined with previous studies of plagioclase that account for the shallowest (10–12 km) parts of the feeding system, allows for a full assessment of the magma dynamics beneath Mt. Etna from 200 ky B.P. to the recent 2011–2012 eruptions. Thermobarometry calculations suggest that cpx crystallization started at about 1380 MPa and continued until magma eruption. The crystallization appears to be continuous in a polybaric vertical feeding system without any evidence of long-lasting magma chambers in the classical sense. The comparison of our results with literature studies confirms that magma crystallization and mineral phase stability are primarily controlled by the concentration of $H_2O$ in basic magmas. Vertical zoning of the physical condition(s) in the feeding system likely occurs due to volatile migration and exsolution that induces a two-stage cpx crystallization. The first stage takes place at great depths where most basic crystals form (>20 km), and the second stage takes place at shallower levels (<20 km) where most of the mixing processes between hydrous and degassed magmas contribute to form the recognized inverse and dusty zoning. Similarly to plagioclase, cpx textural features indicate that periodic injections of basic magmas, with variable water contents, occur within the feeding system, and that magma mingling mostly occurs between 5 and 8 km b.s.l of Mt. Etna. Magma mingling is recorded by reaction textures (dusty rims) and inverse zoning in both cpx and plag, as well as by the occurrence of distinct groups of phenocrysts with more evolved and more basic compositions with respect to the equilibrium composition expected for the host magma. Taken together, both plagioclase and cpx indicate that the feeding system of Mt. Etna volcano is highly dynamic and continuously replenished by mantle-derived magmas.

**Acknowledgments** Authors would like to express thankful to Raul Carampin (CNR-IGG, Unit of Padua) for his support in obtaining quality EMP analysis. Gordon Moore as editor and two anonymous reviewers are greatly acknowledged for guidance and critical suggestions that really improved the original version of the paper. This study was made possible through financial support from MIUR-PRIN Project 2012 (Volatiles transfer at convergent plate margins: linking C–O–H fluids/melts heterogeneities to tectonic anomalies in subduction zones).

## References


Armienti P, Pareschi MT, Innocenti F, Pompilio M (1994) Effects of magma storage and ascent on the kinetics of crystal growth. The case of 1991–93 Mt. Etna eruption. Contrib Mineral Petrol 115:402–414

Armienti P, Tonarini S, D'Orazio M, Innocenti F (2004) Genesis and evolution of Mount Etna alkaline lavas: petrological and Sr–Nd–B isotope constraints. Periodico di Mineralogia 73:29–52

Armienti P, Tonarini S, Innocenti F, D'Orazio M (2007) Mount Etna pyroxene as tracer of petrogenetic processes and dynamics of the feeding system. Geol Soc Am Spec Pap 144:265–276

Armienti P, Perinelli C, Putirka K (2013) A new model to estimate deep-level magma ascent rates, with applications to Mt. Etna (Sicily, Italy). J Petrol. doi:10.1093/petrology/egs085

Blundy J, Cashman K (2001) Magma ascent and crystallization at Mount St. Helens, 1980–1986. Contrib Mineral Petrol 140:631–650

Blundy J, Cashman K (2008) Petrologic reconstruction of magmatic system variables and processes. Rev Mineral Geochem 69:179–239

Bonaccorso A, Bonforte A, Currenti G, Del Negro C, Di Stefano A, Greco F (2011) Magma storage, eruptive activity and flank instability: inferences from ground deformation and gravity changes during the 1993–2000 recharging of Mt. Etna volcano. J Volcanol Geotherm Res 200:245–254

Branca S, Del Carlo P (2004) Eruptions of Mt Etna during the past 3,200 years: a revised compilation integrating the historical and stratigraphic records. In: Bonaccorso A, Calvari S, Coltelli M, Del Negro C, Falsaperla S (eds) Mount Etna: Volcano Laboratory. AGU (Geophys. monograph series), vol 143, pp 1–27

Branca S, Coltelli M, De Beni E, Wijbrans J (2008) Geological evolution of Mount Etna volcano (Italy) from earliest products until the first central volcanism (between 500 and 100 ka ago) inferred from geochronological and stratigraphic data. Int J Earth Sci 97:135–152

Cashman KV (1988) Crystallization of Mount St. Helens 1980–1986 dacite: a quantitative textural approach. Bull Volcanol 50:194–209

Corsaro RA, Pompilio M (2004) Buoyancy-controlled eruption of magmas at Mount Etna. Terra Nova 16:16–22

Crabtree SM, Lange RA (2011) Complex phenocryst textures and zoning patterns in andesites and dacites: evidence of degassing-induced rapid crystallization? J Petrol 52:3–38

Crisp J, Cashman KV, Bonin JA, Hougen SB, Pieri DC (1994) Crystallization history of the Mauna Loa lava flow. J Geophys Res 99:7177–7198

Davidson JP, Dj M, Charlier BLA, Harlou R, Hora JM (2007) Microsampling and isotopic analysis of igneous rocks: implications for the study of magmatic systems. Annu Rev Earth Planet Sci 35:273–311

De Beni E, Behncke B, Branca S, Nicolosi I, Carluccio R, Caracciolo D'Ajello F, Chiappini M (2005) The continuing story of Etna's New Southeast Crater (2012–2014): evolution and volume calculations based on field surveys and aerophotogrammetry. J Volcanol Geotherm Res 303:175–186

Duncan AM, Preston RMF (1980) Chemical variation of clinopyroxene phenocrysts from the trachybasaltic lavas of Mount Etna, Sicily. Mineral Mag 42:765–770

Erikson SC (1985) Oscillatory zoning in clinopyroxenes from the Guide Copper Mine, Phalaborwa, South Africa. Am Mineral 70:74–79

Ferlito C (2011) Bimodal geochemical evolution at Sheveluch stratovolcano, Kamchatka, Russia: consequence of a complex subduction at the junction of the Kuril Kamchatka and Aleutian island arcs. Earth Sci Rev 106:49–69

Ferlito C, Lanzafame G (2010) The role of supercritical fluids in the potassium enrichment of magmas at Mount Etna volcano (Italy). Lithos 119:642–650

Ferlito C, Coltorti M, Cristofolini R, Giacomoni PP (2009) The contemporaneous emission of low-K and high-K trachybasalts and the role of the NE Rift during the 2002 eruptive event. Bull Volcanol 71(575):587

Finetti IR (2005) Depth contour map of the Moho discontinuity in the central Mediterranean region from new crop seismic data. In: Finetti IR (ed) CROP PROJECT. Deep Seismic Exploration of the Central Mediterranean and Italy, pp 597–606

Ghiorso MS, Sack RO (1995) Chemical mass transfer in magmatic processes IV. A revised and internally consistent thermodynamic model for the interpolation and extrapolation of liquid–solid equilibria in magmatic systems at elevated temperatures and pressures. Contrib Mineral Petrol 119:197–212

Ghiorso MS, Hirshmann MM, Reiners PW, Kress VC III (2002) The pMELTS: a revision of MELTS for improves calculation of phase relations and major element partitioning related to partial melting of the mantle to 3 GPa. Geochem Geophys Geosyst. doi:10.1029/2001GC000217

Giacomoni PP, Ferlito C, Alesci G, Coltorti M, Monaco C, Viccaro M, Cristofolini R (2012) A common feeding system of the NE and S rifts as revealed by the bilateral 2002/2003 eruptive event at Mt. Etna (Sicily, Italy). Bull Volcanol 74:2415–2433

Giacomoni PP, Ferlito C, Coltorti M, Bonadiman C, Lanzafame G (2014) Plagioclase as archive of magma ascent dynamics on "open conduit" volcanoes: the 2001–2006 eruptive period at Mount Etna. Earth Sci Rev 138:371–393

Gibb FG (1973) The zoned clinopyroxenes of the Shiant Isles Sill, Scotland. J Petrol 14:201–230

Gillot PY, Keiffer G, Romano R (1994) The evolution of Mount Etna in the light of potassium-argon dating. Acta Vulcanol 5:81–87

Ginibre C, Wörner G (2007) Variable parent magmas and recharge regimes of the Parinacota magma system (N. Chile) revealed by Fe, Mg and Sr zoning in plagioclase. Lithos 98:118–140

Ginibre C, Kronz A, Wörner G (2002) High-resolution quantitative imaging of plagioclase composition using accumulated back-scattered electron images: new constraints on oscillatory zoning. Contrib Mineral Petrol 142:436–448

Hirn A, Nicolich R, Gallart J, Laigle M, and ETNASEIS Scientific Group (1997) Roots of Etna volcano in faults of great earthquakes. Earth Planet Sci Lett 148:171–191

Humphreys MCS, Blundy JD, Sparks RSJ (2006) Magma evolution and open-system processes at Shiveluch volcano: insights from phenocrysts zoning. J Petrol 47:2303–2334

Iezzi G, Mollo S, Torresi G, Ventura G, Cavallo A, Scarlato P (2011) Experimental solidification of an andesitic melt by cooling. Geol, Chem. doi:10.1016/j.chemgeo.2011.01.024

Jeffery AJ, Gertisser R, Troll VR, Jolis EM, Dahren B, Harris C, Tindle AG, Preece K, O'Driscoll B, Humaida H, Chadwick JP (2013) Magma plumbing system of the 2007–2008 dome-forming eruption of Kelut volcano, East Java, Indonesia. Contrib Mineral Petrol 166:275–308

Jochum KP, Stoll B, Herwing K, Willbold M, Hofmann AW, Amini M, Aarburg S, Abouchami W, Hellebrand E, Beate Mocek B, Raczek I, Stracke A, AlardO BC, Becker S, Ducking M, Bratz H, Klemd R, De Bruin D, Canil D, Dalpe C, Danyushevsky L, Eisenhauer A, Gao Y, Snow JE, Groschopf N, Gunther D, Latkoczy C, Guillong M, Hauri E, Hofer H, Lahaye Y, Horz K, Jacob DE, Kasemann SA, Kent AJR, Ludwig T, Zack T, Mason PDR, Meixner A, Rosner M, Misawa K, Nash BP, Pfander J, Premo WR, Sun WD, Tiepolo M, Vannucci R, Vennemann T, Wayne D, Woodhead JD (2006) MPI-DING reference glasses for in situ microanalysis: new reference values for element concentrations and isotope ratios. Geochem Geophys Geosyst 7:1–44

Kahl M, Chakraborty S, Costa F, Pompilio M (2011) Dynamic plumbing system beneath volcanoes by kinetic modeling, and the connection to monitoring data: an example from Mt. Etna. Earth Planet Sci Lett 308:11–22

Kahl M, Chakraborty S, Costa F, Pompilio M, Liuzzo M, Viccaro M (2013) Compositionally zoned crystals and real-time degassing data reveal changes in magma transfer dynamics during the 2006 summit eruptive episodes of Mt. Etna. Bull Volcanol 75:692. doi:10.1007/s00445-013-0692-7

Kamenetsky V, Clocchiatti R (1996) Primitive magmatism of Mt. Etna: insights from mineralogy and melt inclusions. Earth Planet Sci Lett 142:553–572

Kuritani T (1999) Phenocryst crystallization during ascent of alkali basalt magma at Rishiri volcano, northern Japan. J Volcanol Geotherm Res 88:77–97

Lachance GR, Traill JR (1966) Practical solution to the matrix problem in X-ray analysis. Can Spectrosc 11:43–48

Landi P, Métrich N, Bertagini A, Rosi M (2004) Dynamics of magma mixing and degassing recorded in plagioclase at Stromboli (Aeolian Archipelago, Italy). Contrib Mineral Petrol 147:213–227

Lanzafame G, Mollo S, Iezzi G, Ferlito C, Ventura G (2013) Unravelling the solidification path of a pahoehoe "cicirara" lava from Mount Etna volcano. Bull Volcanol 75:703–719

Larsen LM (1976) Clinopyroxenes and coexisting mafic minerals from the alkaline Ilimaussaq intrusion, South Greenland. J Petrol 17:258–290

Le Maitre R (2002) Igneous rocks: a classification and glossary of terms. Cambridge University Press, Cambridge

Lundgren P, Berardino P, Coltelli M, Fornaro G, Lanari R, Puglisi G, Sansosti E, Tesauro M (2003) Coupled magma chamber inflation and sector collapse slip observed with synthetic aperture radar interferometry on Mt. Etna volcano. J Geophys Res 108:2247–2267

McDonough WF, Sun SS (1995) The composition of the Earth. Chem Geol 120:223–253

Metrich N, Rutherford MJ (1998) Low pressure crystallization paths of $H_2O$-saturated basaltic–hawaiitic melts from Mt Etna: implications for open-system degassing of basaltic volcanoes. Geochim Cosmochim Acta 62:1195–1205

Métrich N, Allard P, Spilliert N, Andronico D, Burton M (2004) 2001 flank eruption of the alkali- and volatile-rich primitive basalt responsible for Mount Etna's evolution in the last three decades. Earth Planet Sci Lett 228:1–17

Mollo S, Lanzafame G, Masotta M, Iezzi G, Ferlito C, Scarlato P (2011) Cooling history of a dike as revealed by mineral chemistry: a case study from Mt. Etna volcano. Chem Geol 288:39–52

Mollo S, Blundy JD, Iezzi G, Scarlato P, Langone A (2013) The partitioning of trace elements between clinopyroxene and trachybasaltic melt during rapid cooling and crystal growth. Contrib Mineral Petrol 166:1633–1654

Mollo S, Giacomoni PP, Coltorti M, Ferlito C, Iezzi G, Scarlato P (2015a) Reconstruction of magmatic variables governing recent Etnean eruptions: constraints from mineral chemistry and P–T–$fO_2$–$H_2O$ modelling. Lithos 212–215:311–320

Mollo S, Giacomoni PP, Andronico D, Scarlato P (2015b) Clinopyroxene and titanomagnetite cation redistributions at Mt. Etna volcano (Sicily, Italy): footprints of the final solidification history of lava fountains and lava flows. Chem Geol 406:45–54

Monaco C, Tapponier P, Tortorici L, Gillot PY (1997) Late Quaternary slips rates on the Acireale-Piedimonte normal faults and tectonic origin of Mt. Etna (Sicily). Earth Planet Sci Lett 147:125–139

Morimoto N (1988) Nomenclature of pyroxenes. Mineral Mag 52:535–550

Murru M, Montuori C, Wyss M, Privitera E (1999) The locations of magma chambers at Mt. Etna, Italy, mapped by b-values. Geophys Res Lett 26:2553–2556

Patanè D, Privitera E (2001) Seismicity related to 1989 and 1991–93 Mt. Etna (Italy) eruptions: kinematic constraints by fault plane solution analysis. J Volcanol Geotherm Res 109:77–98

Patanè D, Barberi G, Cocina O, De Gori P, Chiarabba C (2006) Time-resolved seismic tomography detects magma intrusions at Mount Etna. Science 313:821–825

Patanè D, Aiuppa A, Aloisi M, Behncke B, Cannata A, Coltelli M, Di Grazia G, Gambino S, Gurrieri S, Mattia M, Salerno G (2013) Insights into magma and fluid transfer at Mount Etna by a multiparametric approach: a model of the events leading to the 2011 eruptive cycle. J Geophys Res 118:3519–3539

Peccerillo A, Lustrino M (2005) Compositional variation of Plio-Quaternary magmatism in the circum-Tyrrhenian area: deep versus shallow mantle processes. In: Foulger GR, Natland JH, Presnall DC, Anderson DL (eds) Plates, plumes, and paradigms: Geol Soc Amer Spec Paper, vol 338, pp 421–434

Phemister TC (1937) A review of the problems of the Sudbury Irruptive. J Geol 45:1–47

Putirka KD (2008) Thermometers and barometers for volcanic system. In: Putirka KD, Tepley F (eds) Minerals, inclusions, and volcanic processes: Rev Min Geochem, vol 69, pp 61–120

Putirka K, Johnson M, Kinzler R, Walker D (1996) Thermobarometry of mafic igneous rocks based on clinopyroxene–liquid equilibria, 0–30 kbar. Contrib Mineral Petrol 123:92–108

Putirka K, Ryerson FJ, Mikaelian H (2003) New igneous thermobarometers for mafic and evolved lava compositions, based on clinopyroxene + liquid equilibria. Am Mineral 88:1542–1554

Schiano P, Clocchiatti R, Ottolini L, Busà T (2001) Transition of Mount Etna lavas from a mantle-plume to an island-arc magmatic source. Nature 412:900–904

Sharp ADL, Davis PM, Gray F (1980) A low velocity zone beneath Mount Etna and magma storage. Nature 287:587–591

Tanguy JC, Condomines M, Kieffer G (1997) Evolution of Mount Etna magma: constraint on the present feeding system and eruptive mechanism. J Volcanol Geotherm Res 75:221–250

Tsuchiyama A (1985) Dissolution kinetics of plagioclase in the melt of the system diopside–albite–anorthite, and the origin of dusty plagioclase in andesites. Contrib Mineral Petrol 89:1–16

Vetere F, Iezzi G, Behrens H, Holtz F, Ventura G, Misiti V, Cavallo A, Mollo S, Marcel D (2015) Glass forming ability and crystallization behaviour of sub-alkaline silicate melts. Earth Sci Rev 150:25–44

Viccaro M, Ferlito C, Cortesogno L, Cristofolini R, Gaggero L (2005) Magma mixing during the 2001 event at Mount Etna (Italy). Effects on the eruptive dynamics. J Volcanol Geotherm Res 149:139–159

Viccaro M, Giacomoni PP, Ferlito C, Cristofolini R (2010) Dynamics of magma supply at Mt. Etna volcano (Southern Italy) as revealed by textural and compositional features of plagioclase phenocrysts. Lithos 116:77–91